J Mater Sci (2017) 52:3657–3669

Batteries and Supercapacitors

Polymer/ceramic co-continuous nanofiber membranes via room-curable organopolysilazane for improved lithium-ion battery performance

Soshana A. Smith[1], Jay Hoon Park[2], Brian P. Williams[2], and Yong Lak Joo[2,*]

[1] Department of Fiber Science and Apparel Design, Cornell University, Ithaca, NY 14853, USA
[2] School of Chemical & Biomolecular Engineering, Cornell University, Ithaca, NY 14853, USA

Received: 28 July 2016
Accepted: 7 November 2016
Published online: 21 November 2016

ABSTRACT

Polyacrylonitrile (PAN) and ambient temperature-curable organopolysilazane were combined to successfully fabricate PAN/polymer-derived ceramic (PDC) hybrid nanofiber separator using a single-step electrospinning process. The amount of added precursor was varied from 10 to 30% to characterize the effects of various loadings on the mechanical, thermal properties, and electrochemical performance on the hybrid membranes. TEM images reveal that all composite fibers have a thin (~5 nm) ceramic-rich sheath layer surrounding each fiber. In addition, there is also ceramic present inside the fiber with the ceramic forming continuous network within the nanofiber at high concentrations. The interconnected ceramic network within the fiber disrupts the polymers ability to properly crystallize, leading to an increase in amorphous regions with an increase in ceramic inclusion. The presence of the ceramic on the surface of the membrane in addition to the increased amorphous regions leads to excellent ionic conductivity and cycling performance. The 30 wt% PDC sample has an ionic conductivity of 1.05 mS cm^{-1} compared to 0.29 mS cm^{-1} of pristine PAN separator. All separators with additional PDC content showed increased initial capacity and capacity retention at 0.2C charging and discharging rate, with the 90:10, 80:20, and 70:30 wt% of PAN:PDC showing 89, 90 and 93% capacity retention of graphite/$LiCoO_2$ full cells over 100 cycles, respectively. In rate capability testing, PAN/PDC fibers demonstrated increased capacity retention even at increased charge rates. The results suggest that the increased ionic conductivity and wetting behavior by both the ceramics within the membrane and on the surface of the membrane are more correlated to an increase in capacity retention and rate capability than the porosity.

Address correspondence to E-mail: ylj2@cornell.edu

DOI 10.1007/s10853-016-0574-4

Introduction

Lithium-ion batteries are used worldwide in a variety of electronic devices due to their high energy density, high efficiency, and long life cycle [1]. A separator plays a key role within the battery, acting as a physical barrier between the cathode and the anode, while aiding in ionic transport. An ideal separator should allow for the rapid transport of ionic charge carriers while maintaining good thermal and mechanical stability as well as being chemically inert [2]. Current commercially available polyolefin separators fulfill some of the previously mentioned criteria, but they also possess many disadvantages. Due to the intrinsic hydrophobic nature of polypropylene and polyethylene polymers used to manufacture the separators, the separators have low wettability and electrolyte uptake [3]. In addition to low wettability, polyolefin separators have low porosity approximately 40–50%, limiting the ion transport pathway [1]. These combined factors of poor wettability and low porosity lead to poor ionic transport over the lifetime of the batteries containing polyolefin separators.

Interest in non-woven separators has risen over the last decade to overcome some of the shortcomings of the polyolefins [4–7]. Micron and sub-micron nonwoven membranes can be made using a variety of methods including centrifugal spinning [8, 9], force spinning [10, 11], electrospinning [12–14], among others. While the former two techniques have a high throughput of materials, it is still currently difficult to properly control the fiber and membranes morphology. Yanilmaz et al. [8, 15] showed fiber diameters up to 10 microns, up to ten times that of typical fibers produced via the electrospinning process. Electrospinning results in fibers well below the sub-micron scale with a narrower fiber diameter distribution compared to other methods. Using the electrospinning method, nonwoven separators have been fabricated from a variety of polymers including polyethylene terephthalate (PET) [16], polyacrylonitrile (PAN) [17, 18], polyvinylidene fluoride (PVDF) [19, 20], meta-aramid [21], and polyimide (PI) [22]. The porous 3-D structure of the electrospun fiber network resulted in a dramatic increased the porosity of separator membranes from 40–50 to 60–80%. This increase in porosity is correlated with an increase in ionic conductivity due to a higher effective diffusivity of the electrospun membranes. In addition, using more hydrophilic polymers instead of hydrophobic olefins allows for greater uptake of the electrolyte solution and better electrolyte retention in the batteries. Due to the increased porosity and increased wettability, nonwoven separators showed increased initial recharge capacity and capacity retention compared to the commercial polyolefin separator, Celgard [23, 24].

To further improve the performance of separators, researchers are also including ceramic components, such as SiO_2 and Al_2O_3 to non-woven separators [25–28]. The inclusion of ceramics resulted in composite separators with good ionic conductivity, high thermal stability and improved cycling performance [29, 30]. The inclusion of ceramics into nonwovens is usually done via three methods: incorporating the ceramic directly into the polymer [18], coating the non-woven in a ceramic [31], or a multilayer rolling process [32]. Jung et al. incorporated fumed silica into PAN fibers to form separators with excellent cycling performance but could only improve electrochemical performance up to 12 wt%. Due to issues with dispersion of the silica within the PAN matrix, there was a limit to the enhancements from the silica particles. The coating and rolling methods also enhanced the battery performance. However, using either the rolling or coating method often results in either delamination of the ceramic from the polymer or a phase separation which negates any benefits of adding a ceramic component.

In this work, a polymer/ceramic non-woven separator is created in a one-step electrospinning process similar to Jung et al. Combining ceramics such as SiO_2 and nanoclay into polymer solutions usually require extensive ultra-sonication to achieve good dispersion of the inorganic ceramic within the fiber due to their tendency to aggregate. However, organopolysilazane is 100% miscible with PAN, thus allowing uniform distribution of PDC along the fiber axis without the need for an additional preparation process. By combining PAN with a ceramic precursor, we were able to produce polymer/ceramic hybrid nanofiber separators at room temperature with high ceramic loading with no need for ultrasonication or any further post-treatment processes. In addition, incorporating the ceramic directly into the nanofiber eliminates any issues of phase separation or delamination of the two components, a major drawback of the previous works using multilayer hybrid ceramics. In this work, we varied the amount

of precursor to demonstrate the effect of ceramic content on cycling performance compared to a pure PAN non-woven separator. We also present how an increase in ceramic content leads to an increase in ionic conductivity, initial capacity, and overall capacity retention over the lifetime of the battery.

Experimental section

The PAN/ceramic non-woven separator was prepared using the electrospinning method. The electrospinning solution was prepared by combining Polyacrylonitrile (PAN, $M_W = 200{,}000$, Polysciences) with *N*,*N*-dimethylformamide (DMF) to form a 8 wt% solution. The solution was placed in a 95 °C oven for 12 h to thoroughly dissolve the polymer. The PAN/DMF was then left to cool at room temperature for 1 h. The ceramic precursor, organopolysilazane (OPSZ, EMD Performance Materials), was added to obtain the desired weight percentage (10, 20 and 30 wt%) in relation to PAN. The mixture was stirred on a vortex mixer for 2 min to ensure thorough mixing of the components. The solution was left sitting for 10 min to allow any bubbles within the solution to disappear before spinning the solution.

The PAN/OPSZ solution was electrospun at a flow rate of 0.9 mL h^{-1} for the 10 and 20 wt% solution and 0.6 mL h^{-1} for the 30 wt% solution using a 20-gauge needle. A 17.5 kV voltage and 15 cm distance between the needle and the collector plate were used for all samples. The collected samples were then annealed at 120 °C for 12 h to ensure the removal of all residual solvent.

Material characterization

The presence of ceramic elements in the final fiber was determined using Fourier transform infrared spectroscopy (FTIR) under ambient conditions within the range of 700–4000 cm^{-1} with a resolution of 4 cm^{-1} for 512 scans. The fiber morphology and diameter were examined using scanning electron microscopy (Tecsa Mira3 Field Emission SEM) with an accelerating voltage of 5 kV. The average fiber diameters were determined by choosing 100 randomly selected fibers using Image J. The morphology of the cross-section of the fibers was investigated by transmission electron microscopy (FEI Tecnai G2 T12 Spirit TEM STEM). Ceramic content was approximated using thermogravimetric analysis (TGA) under nitrogen from 25 to 1000 °C at a 10 °C heating rate. Thermal stability was characterized using differential scanning calorimetry (DSC, TA Instrument Q200) under nitrogen from 40 to 350 °C at a 10 °C heating rate. Wide-angle X-ray diffraction (XRD) patterns were recorded from 10° to 70° for all prepared electrospun membranes using theta–theta X-ray diffractometer (Scintag) with Cu radiation ($\lambda = 1.5405$ Å; 40 mA and 40 kV). The separator/electrolyte interaction was estimated by measuring the dynamic change in contact angle between the electrolyte and the separator using a high-speed camera capturing images every 0.001 s. Electrolyte uptake is calculated using the following relation:

$$\text{Uptake } (\%) = \frac{M_a - M_i}{M_i} \times 100 \quad (1)$$

where M_a and M_i are the masses of the wet and dry membrane, respectively. The porosity (P) of the fabricated membranes was calculated using the measured data and the density of material with the equation below [33].

$$P = 1 - \left(\frac{W}{\rho \cdot V}\right) \quad (2)$$

where W is the dried membrane weight, ρ the membrane density, and V the apparent volume of the membrane. The membrane thickness was measured by a digital thickness gauge. A capillary flow porometry (Porous Media Inc., NY) was used to characterize pore size distribution of the fabricated membranes from the dry and wet flow curves.

Electrochemical characterization

Electrochemical tests are carried out in 2032 coin cells. Cell impedance was measured by sandwiching the separator membrane between two lithium disks inside a cell. The cells were tested on a PARSTAT 4000 (Princeton Applied Research), with the impedance measurements at an amplitude of 5 mV over a frequency range of 20,000 kHz–1 Hz.

Full cell consisted of a graphite anode (MTI Corporation), a $LiCoO_2$ cathode (MTI Corporation), and $LiPF_6$-EC/DMC/DEC electrolyte; cycling was carried out at a voltage range between 2.5 and 4.2 V at a 0.2C charge and discharge rates. Discharge rate capabilities were tested by charging cells to 4.2 V at 0.1C rate for

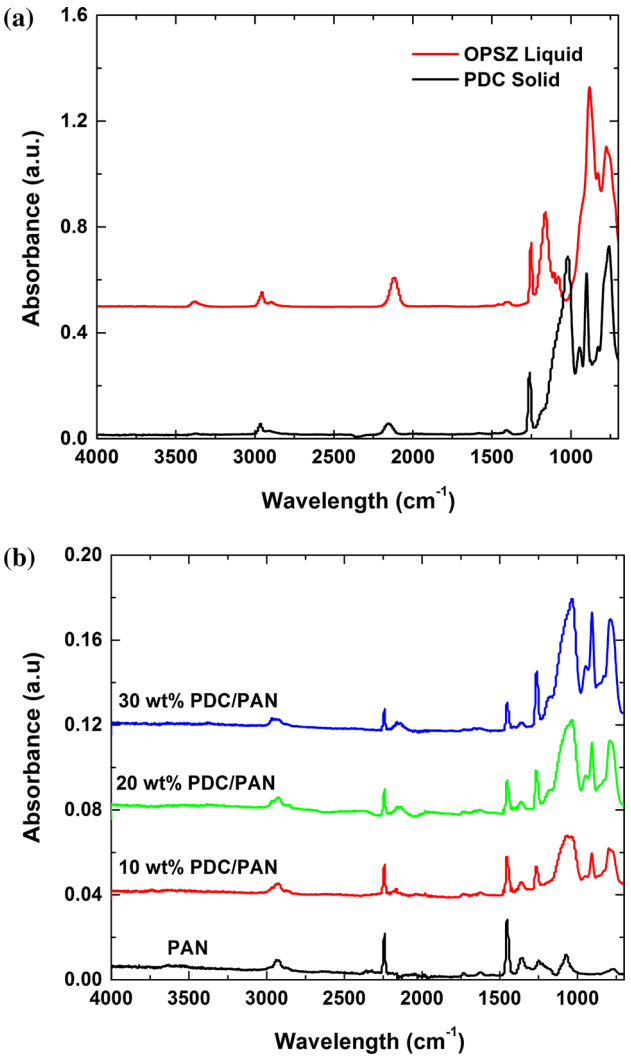

Figure 1 **a** FTIR spectra of liquid OPSZ and cured PDC **b** FTIR spectra of PAN and PAN/OPZ electrospun membrane.

the first and last cycles and 0.2C rate for all other cycles. Cells were discharged at 0.1, 0.2, 0.5, 1, 2, 5, and 0.1C, respectively.

After cycling, cells were taken apart to analyze the post-cycling morphology of the membranes. The used separators were rinsed in DMC solution and left to sit in fresh DMC solution overnight to remove any debris from the membrane surface.

Results and discussion

Physical properties

FTIR results of the uncured OPSZ liquid (Fig. 1a) reveal the following characteristic peaks: Si–NH–Si bending mode at 1159 cm^{-1}, NH stretching mode at 3380 cm^{-1}, and a doublet peaks 1104 and 1074 cm^{-1} indicating the presence of $SiOCH_2CH_3$. The liquid precursor was left at ambient temperature open to air for 3 weeks to cure via moisture cure crosslinking. Once the liquid is fully cured, the peaks at 1159 and 3380 cm^{-1} disappear. Additionally, a peak at 1037 cm^{-1} indicating a Si–O–Si stretching mode is present in the cured sample, while the peak at 812 cm^{-1} consistent with the bending mode of the Si–O–Si bond is also present. The peak shifts from the OPSZ liquid to the PDC indicating that the liquid is able to undergo a crosslink curing with itself at ambient conditions. After electrospinning PAN and OPSZ, the FTIR results of the PAN/PDC fibers can be seen in Fig. 1b. All samples contain a peak at 1037 cm^{-1} indicating the presence of Si–O–Si within the fiber. Furthermore, the absence of peaks at 1159, 3380, 1104, and 1074 cm^{-1} shows that the OPSZ has undergone both a TEOS reaction and the Si–N reaction along the backbone of the fiber. During the electrospinning process, the OPSZ precursor was able to react with water in the air to cure into a PDC. These results show that we have successfully made PAN/PDC nanofibers.

It is important that a non-woven separator membrane has uniform fiber morphology to ensure the best performance. The morphology of the non-woven fibers can be seen in Fig. 2. SEM images of the non-woven mat show that the separator consists of porous networks composed of uniform, well-formed nanofibers. The fiber diameters range from approximately 390 to 450 nm, with the fiber diameter slightly increasing with the increased ceramic content (Fig. 2).

TEM images (Fig. 3) shows the distribution of polymer-derived ceramic within the PAN polymer matrix. All three examples show a phase-separated hybrid system with the ceramic phase well distributed across the cross-section of the fiber. As the concentration of ceramic increases, the domain sizes increase from an average of 10 nm for the 90/10 wt% fiber (Fig. 3a, b), 25 nm for the 80/20 wt% (Fig. 3c, d) to 40 nm for the 70/30 wt% fiber (Fig. 3e, f). For the lowest ceramic loading, the larger particles are located toward the center and get smaller in diameter along the radius. In 80/20 wt% fibers, particle sizes become larger and more uniform across the fiber diameter. As the concentration of OPSZ increases, there are more opportunities for the organopolysilazane to complete the moisture cure reaction,

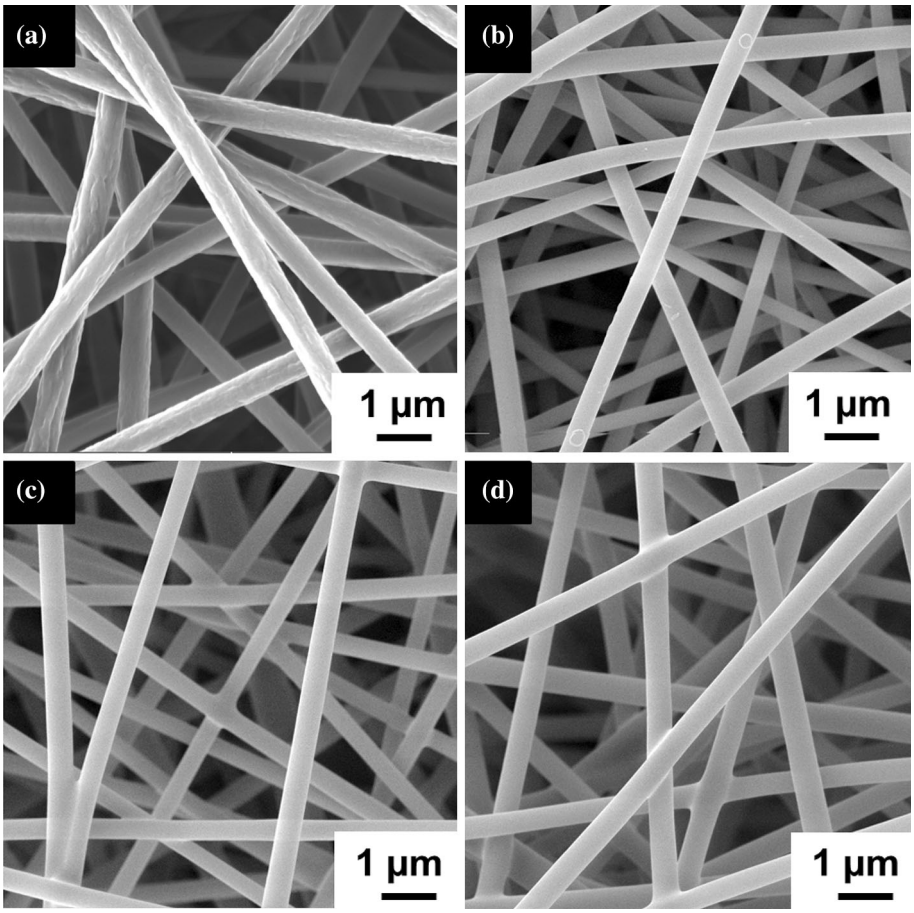

Figure 2 SEM images of electrospun membranes. **a** PAN **b** PAN/PDC 90:10 wt% **c** PAN/PDC 80:20 wt% **d** PAN/PDC 70:30 wt%.

resulting in larger particles. This is confirmed in the 70/30 wt% sample (Fig. 3e, f), with the particles appearing larger and more elongated along the fiber axis compared to the two previous samples. For all loadings, there is a thin, 4–6 nm sheath layer on the outside of each nanofiber as seen in the TEM images. A HR-TEM image (Fig. 3g) of the edge of a fiber clearly shows the proposed ceramic sheath layer, followed by a ceramic-free layer eventually leading to the ceramic domains toward the center. XPS analysis (Fig. 4) reveals that this thin layer is rich in silicon and oxygen indicating the ceramic has formed a sheath layer around each fiber during the electrospinning process. Having ceramic both on the inside and on the surface of the polymer created a unique morphology that cannot be easily recreated with the use of previously commonly used ceramic nanoparticles.

Using DMF, the PAN from the composite was removed to reveal the ceramic structure within the fiber. For the 10 wt% loading, the ceramic forms small discrete domains as seen in Fig. 5a. However, as the ceramic content increases the ceramic domain forms a continuous network independent of the polymer matrix. In Fig. 5b and c, SEM images reveal that the ceramic still maintains a fibrous structure, proving the ceramic portion forms its own interconnected domain. The ceramic domain also appears to be porous, suggesting the ceramic and polymer network are intertwined along the fiber axis. At high loadings, the inclusion of PDC leads to a unique co-continuous polymer/ceramic nanofiber morphology.

TGA analysis was used to confirm both the weight percent inclusion of PDC in the nanofibers and to demonstrate the thermal stability of the non-woven membranes. The TGA results shown in Fig. 6a indicate that there are 26, 17, and 8% residual materials after 1000 °C for the 30, 20, and 10 wt% samples, respectively. These results confirm that the OPSZ precursor material fully converted to a ceramic during the electrospinning and annealing processes. DSC results (Fig. 6b) show that the inclusion of PDC also has an effect on the onset of cyclization of the PAN

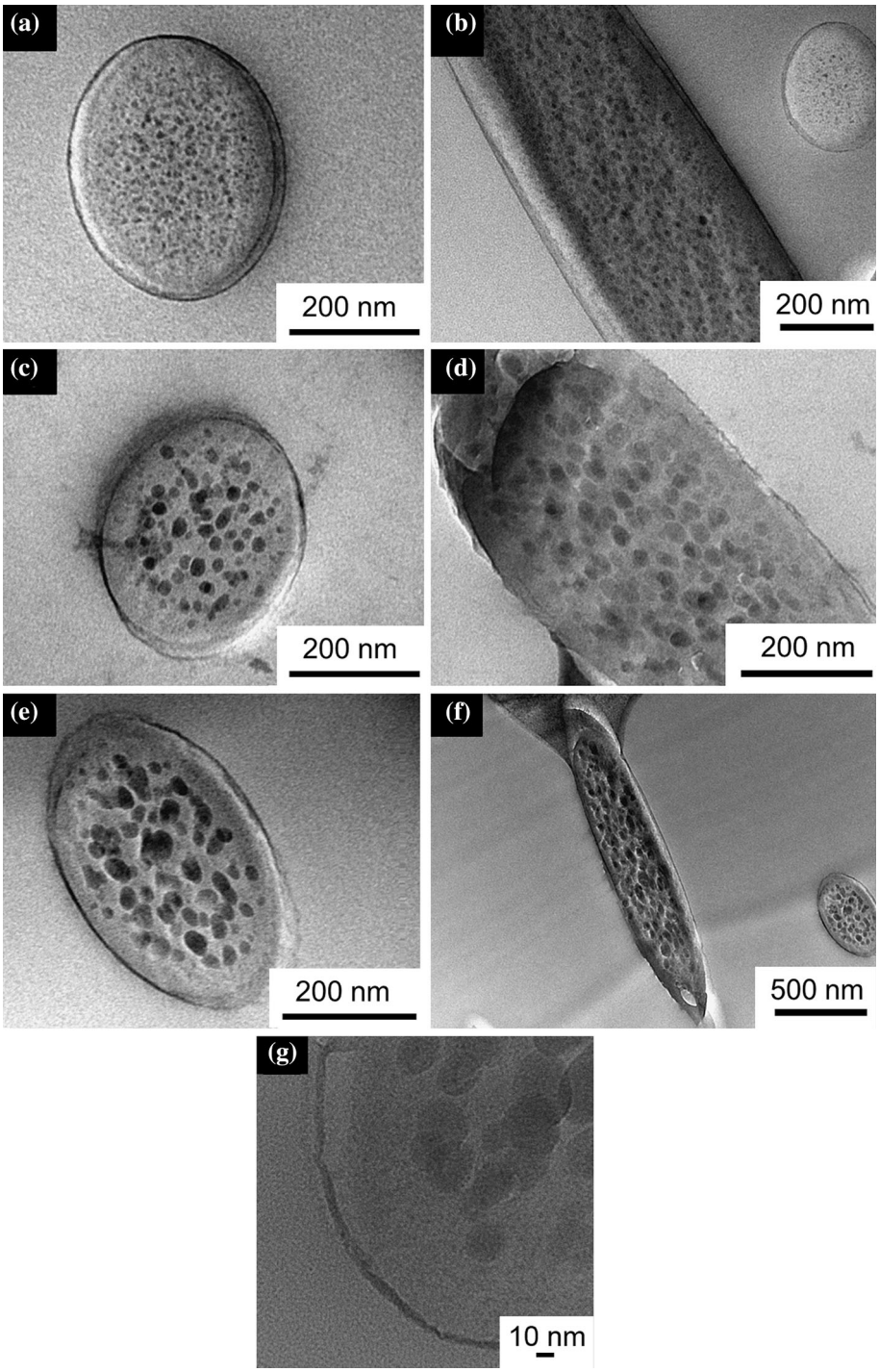

Figure 3 TEM images of PAN/OPZ composite fibers. **a**, **b** Fiber cross-section and along the fiber axis of 10 wt% fibers. **c**, **d** Fiber cross-section and along the fiber axis of 20 wt% fibers. **e**, **f** Fiber cross-section and along the fiber axis of 30 wt% fibers. **g** HR-TEM images of edge of a fiber clearly showing the sheath layer surrounding the fiber.

polymer. Pure PAN had a cyclization temperature (T_c) of 291 °C, while the 90/10 wt% and 80/20 wt% fibers have T_c of 294 and 296 °C, respectively. This shows that the ceramic in having a positive interaction with the polymer network. Similar to previously studied polymer/ceramic matrices, PDC enhances the thermal stability of the polymer matrix [34, 35]. The increase in cyclization temperature is thought to be a result of the ceramic inhibiting the formation and escape of volatile byproducts generated during the dehydrogenation of PAN. However, as the ceramic inclusion increases to 30 wt%, T_c decreases back to

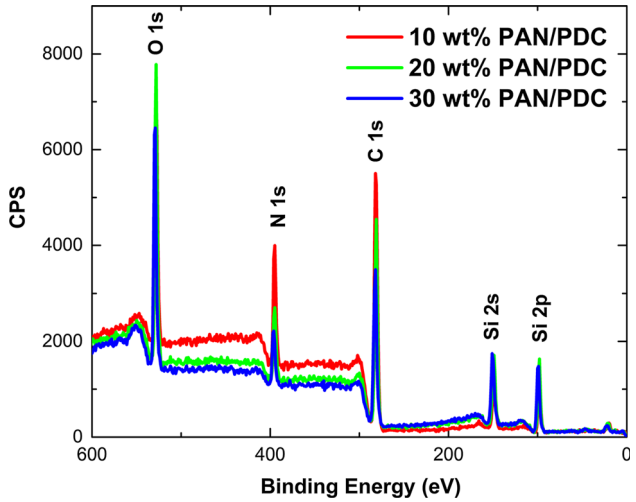

Figure 4 XPS spectra of various PAN/PDC membranes showing the presence of silicon- and oxygen-rich ceramic layers on the surface of the fibers.

292 °C. This behavior suggests that the ceramic and the polymer are now acting as two separate components with no interaction between the two domains.

In addition to improved thermal stability, good mechanical stability is a desired property of separators for electrochemical applications. Figure 7 shows the typical stress/strain curve of PAN and PAN/PDC membranes at various loadings. Young's modulus increased at all loading compared to the pristine PAN membrane, increasing from 101 ± 26 MPa for the PAN separator to 343 ± 32 MPa for the 30 wt% loading. In addition for all loadings, there is an increase in stress at break. However, it is clear that there is a limit on how much ceramic can be added to improve the stress at break. The 20 wt% membrane has a stress at break three times that of pristine PAN. However, as the loading increases to 30 wt%, the membrane begins to exhibit brittle behavior due to the high ceramic loading. The 30 wt% sample breaks at the yield point, exhibiting no ductile behavior. Even considering this drawback, the 30 wt% membrane still has superior strength compared to the PAN membrane.

Figure 8 shows the XRD patterns of the PAN membrane as well as the PAN/PDC membranes with various ceramic loadings. The XRD pattern of the pure PAN membrane shows a strong peak at 17° and a weak broad peak at 28°; the peak at 17° corresponds to (0 1 0) plane with d spacing of 5.3 Å [36, 37]. As more ceramic is added, the peak at 17° becomes weaker and the peak at 28° disappears. This indicates that the inclusion of PDC ceramic enhances the amorphous phase of the PAN polymer.

How well a separator wets with electrolyte is a good indication of how well the electrolyte is diffusing in the separator and also how effectively the separator can retain electrolyte [3]. Figure 9 shows the dynamic contact angle measurements of the Celgard, PAN, and the PAN/PDC nonwoven membranes. All nonwoven membranes show superior electrolyte uptake due to increased porosity. The hydrophobic nature of the PDC ceramic works well with the organic EC/DMC/DEC electrolyte used in the system to create a more favorable interaction between the separator and electrolyte. As time increases, the contact angle between the PAN/PDC separators is decreasing more rapidly than the PAN separator. This indicates better absorption of the electrolyte into the pores of the polymer/ceramic separators. Comparing the PAN/PDC samples, it is clear that an increase in ceramic material also correlates with a decrease in contact angle. Improved polymer membrane/electrolyte interaction is further evidenced in Fig. 9b with electrolyte uptake results. The electrolyte uptake of microporous polyolefin membrane is 148% which is more than 5 times less than that of the pure PAN sample. The low porosity (~42%)

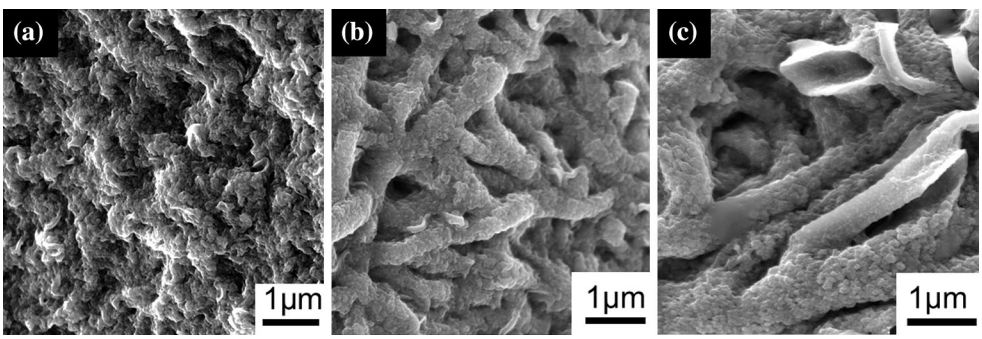

Figure 5 SEM images of fiber mats after PAN has been removed with DMF. **a** 10 wt%, **b** 20 wt%, **c** 30 wt%.

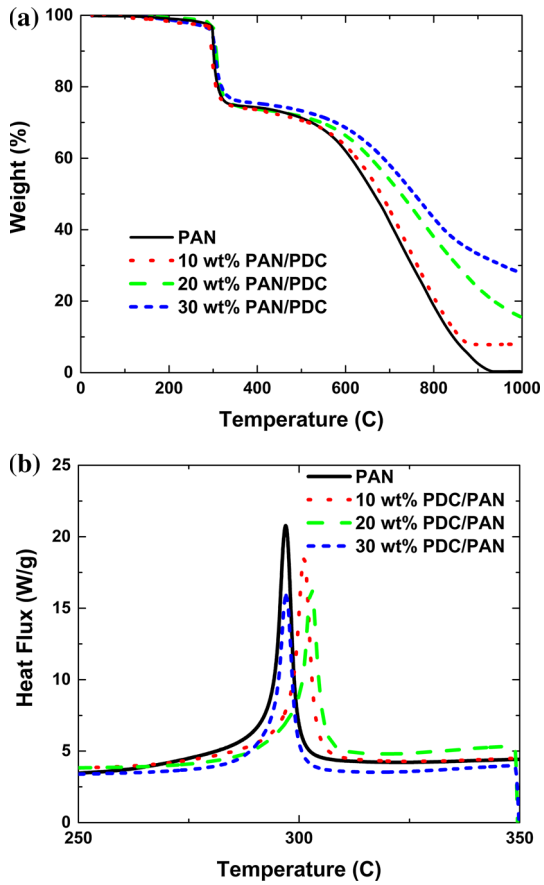

Figure 6 **a** TGA isotherms of PAN and PAN/PDC mats. **b** DSC measurement showing the cyclization temperature, an exothermic process, of the PAN polymer.

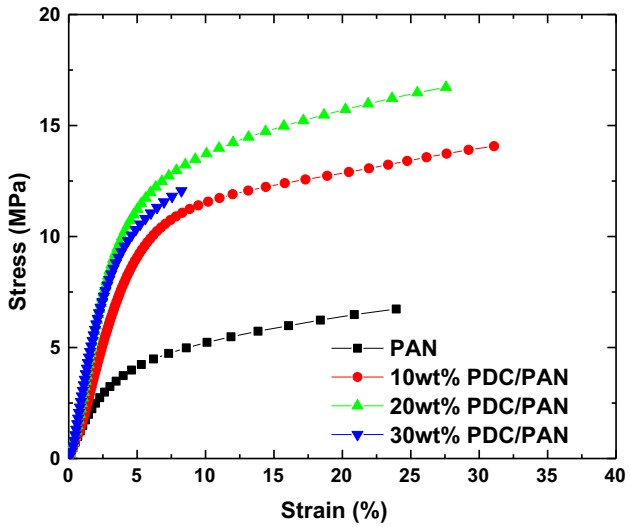

Figure 7 DMA showing the mechanical stability of PAN and PAN/PDC membranes.

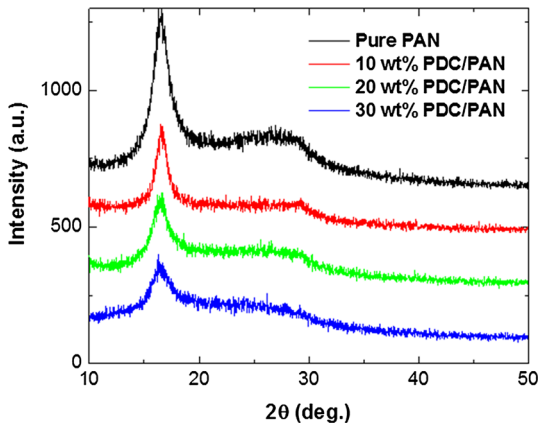

Figure 8 XRD patterns of electrospun PAN/PDC composite membranes with various ceramic contents.

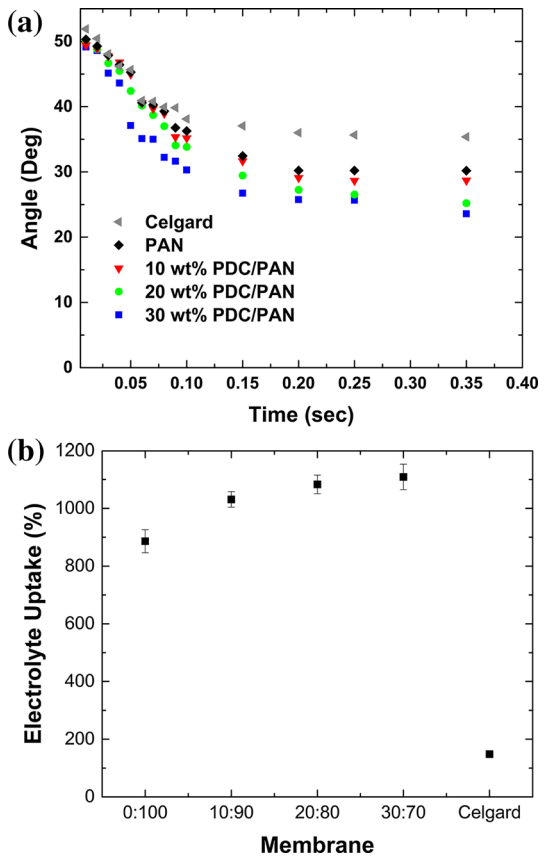

Figure 9 **a** Dynamic contact angle measurements as a function of time using various membranes. **b** Variations of electrolyte uptake in electrospun PAN/PDC composite membranes with PDC content.

of the polyolefin membrane and the hydrophobic nature of the polymers lead to its low electrolyte uptake. However, the high porosity of the PAN and PAN/PDC (see Table 1) increases the uptake significantly by being able to trap and retain more

Table 1 Characteristics of PAN/PDC composite separators of various PDC inclusions

	Fiber diameter (nm)	Pore size distribution (nm)	Porosity
PAN	439 ± 48	358 ± 58	82
PAN/PDC 90:10	390 ± 74	843 ± 76	83
PAN/PDC 80:20	392 ± 50	463 ± 72	80
PAN/PDC 70:30	490 ± 66	423 ± 100	82

electrolytes. Comparing the PAN and the PAN/PDC membranes, there is an increase in the electrolyte uptake with increased ceramic content. This is due to an increase in the amorphous regions of the PAN polymer. The inclusion of ceramic significantly affects the PAN polymer's ability to crystallize (Fig. 8) leading to an increase in the amorphous regions of the polymer and hence an increase in electrolyte uptake. The ceramic present in the membranes is also amorphous, and thus, solely increasing the amount of ceramic increases the overall amorphous content of the membrane (Fig. 8).

Electrochemical performance

The ionic conductivity of a Li-ion separator helps with the transport of ions during the charge–discharge process of the batteries. The Nyquist plot of the results for all separators can be seen in Fig. 10. The high-frequency intercept of the semi-circle with the *ZRe* intercept represents the bulk resistance, R_b. Since the graph does not have any intercept, the curve is fitted using Zview using the equivalent circuit as seen in the inset. Ionic conductivity can then be determined using

$$\delta = \frac{d}{S \times R_b} \tag{3}$$

where δ is ionic conductivity, d is the thickness of the separator membrane, S is the area of the lithium electrode, and R_b is the bulk resistance. The calculated ionic conductivities of all separators tested are displayed in Table 2. Similar to previous works, the ionic conductivity of PAN is improved compared to Celgard 2400 due to increased porosity and electrolyte uptake. The results show that the PAN/ceramic separators have a higher ionic conductivity compared to the PAN electrospun membrane. As the concentration of PDC increases, there is an increase in the ionic conductivity, with the 70 wt% PAN/PDC separator having an ionic conductivity value three times that of the plain PAN separator membrane. Increase in ionic conductivity due to ceramic inclusion has been well documented [38–40]. The increase in ionic conductivity can be attributed to a number of factors including: pore structure within the membrane to trap the electrolyte, increase in amorphous regions of the polymer due to inorganic inclusion, and ceramics acting as the Lewis acid–base center that promotes salt disassociation which could free more cations [39, 40]. The pore sizes of 70 wt% PAN/PDC membrane being the smallest among the polymer/ceramic samples enabled it to provide good ionic channels and high liquid electrolyte uptake in pores without leakage. The membranes with the highest ceramic content also have the lowest

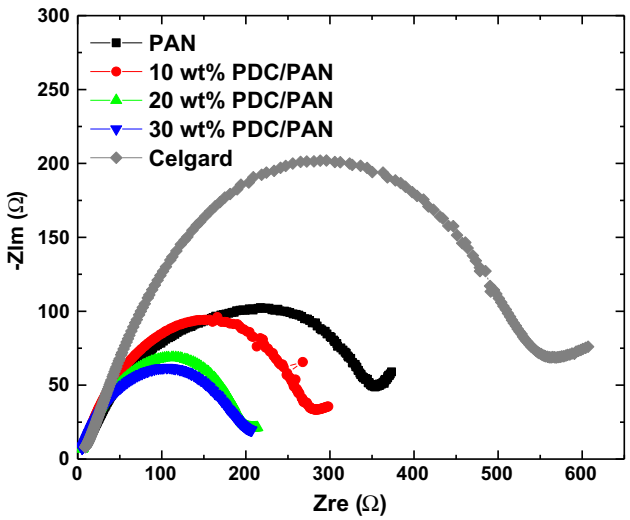

Figure 10 Nyquist plots for the cells with Celgard, PAN membrane, 90:10 wt%, 80:20 wt%, 70:30 wt% PAN/PDC membranes, respectively.

Table 2 Electrochemical impedance spectra (EIS) of various separators

Membrane	Ionic conductivity (mS cm^{-1})
Celgard	0.22
PAN	0.29
PAN/10 wt% PDC	0.51
PAN/20 wt% PDC	0.80
PAN/30 wt% PDC	1.14

crystallinity and highest electrolyte uptake, leading to the increase in ionic conductivity. In addition, the ceramic-rich sheath layer is able to directly interact with the lithium salt to promote salt dissociation leading to higher ionic conductivity.

Figure 11 shows the discharge capacity of graphite/$LiCoO_2$ full cells using various separators. Figure 11a shows the cycling performance at a 0.2C rate. The initial discharge capacity for Celgard was 131 mAh g^{-1}, while the initial discharge capacity for the PAN/PDC cells were 135 mAh g^{-1}. Over the life cycle of the battery, Celgard had the capacity retention of 85% after 100 cycles. We note that despite doubling the porosity (41% vs. 82%), the performance of PAN nanofiber separator (86% retention) was very close to that of Celgard suggesting that Li-ion transfer through the pores may not be a deciding factor to enhance the performance of the separator. Meanwhile, the PAN/PDC membranes had higher capacity retentions of 89, 90, and 93% for the 10, 20 and 30 wt% PAN/PDC membranes. Increase in initial capacity and capacity retention can be attributed to the increased electrolyte uptake and ionic conductivity caused by ceramic inclusion. When the charge rate is increased to 0.5C, a similar trend is seen in Fig. 11b. The membrane with the highest ceramic loading, 30 wt%, maintained a 91% capacity retention after 100 cycles. The pure PAN membrane is only able to maintain an 80% capacity retention, and the Celgard membrane performance has the poorest performance with a 63% capacity retention after 100 cycles.

Rate capability of cells with various separators can be seen in Fig. 12. Similar to the 0.5C testing, PAN/PDC cells begin with a higher initial discharge capacity, 135 mAh g^{-1} for the PAN/PDC 70:30 wt% cell compared to 128 mAh g^{-1} for the PAN cell. As the cycling continues, PAN/PDC separators continuously exhibit an average 10 mAh g^{-1} improvement over the PAN separator. PAN/PDC separators demonstrate very stable cycling behavior over a range of charge rates maintaining over a 90% retention of the 0.1C capacity at 1C, while the PAN cell has fallen to 80% retention at 1C. As the charge rate is increased to 5C, the rate retention rates are 38, 41, 53, and 53% for the PAN, PAN/PDC 90:10, 80:20, and 70:30 wt% cells, respectively. As the cells are brought back to a gentler cycling rate, 0.1C, it is clear that the separator is used as an impact on the battery's ability to recover after such a high charge rate. The PDC samples all immediately regain discharge capacities similar to the capacities at 0.2C charge rate, approximately 90% of the initial C/10 capacity. While the PAN separator is only able to recover to a previous 1C conditions, with a 105 mAh g^{-1} capacity, 80% of the initial C/10 capacity. It should be noted that despite similar porosity values (80–83%) for all nanofiber-based separators in the current study, the presence of ceramic in the fiber

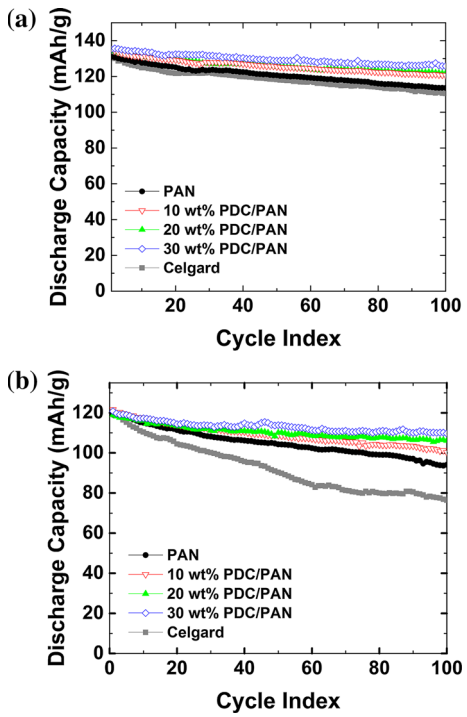

Figure 11 Cycle performance of $LiCoO_2$/graphite full cells with various separator membranes at 0.2C.

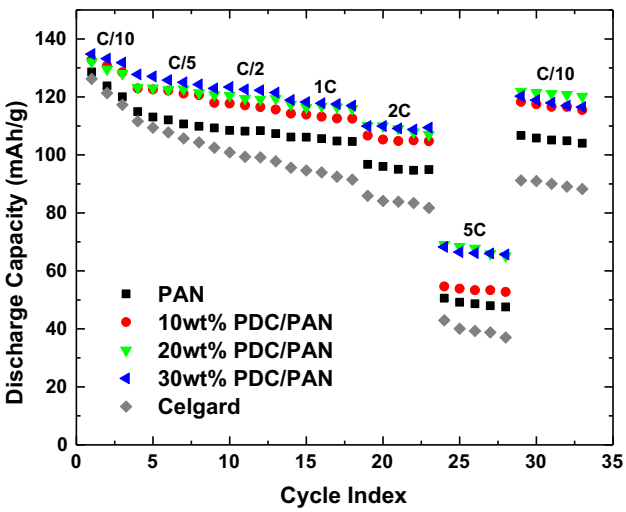

Figure 12 Results of rate capability tests for the $LiCoO_2$/graphite full cells with various separator membranes.

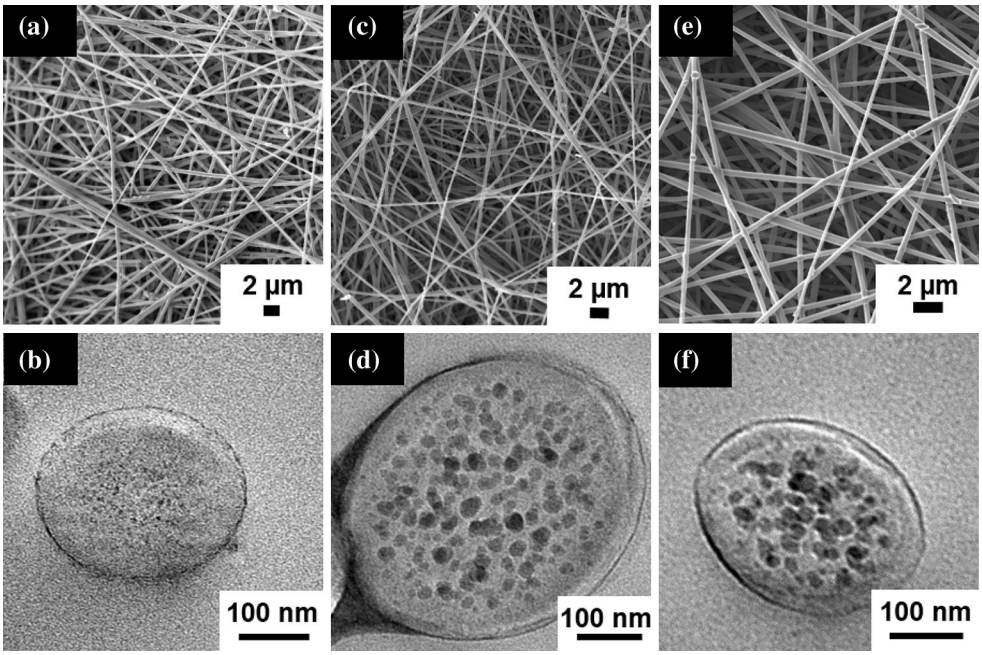

Figure 13 SEM and TEM images of post-mortem PAN/PDC fibers after cycling showing they retain their morphology. **a**, **b** 10 wt%, **c**, **d** 20 wt%, **e**, **f** 30 wt%.

greatly improved the rate capability performance suggesting that the ionic conductivity and wettability becomes more important than the porosity for better separator performance.

Analysis of the membranes after cycling reveals that the membranes maintain their internal and external morphologies after *C*-rate testing (Fig. 13). SEM images of post-mortem membranes (Fig. 13 a, c, e) show that the membranes have maintained their morphology with no evidence of broken fibers. In addition, there appears to be no change in the pore structure of the membranes. Comparing the post-cycling images to pristine fibers in Fig. 3, it shows little difference in the cross-section of the fibers. This shows that the hybrid membranes are not affected by the harsh conditions within the Lithium-ion battery full cell. TEM images of the membranes show that the ceramic sheath layer is still intact after strenuous 5C cycling conditions. A current drawback of the use of nanoparticles on the surface of separator membranes is the delamination of the particles from the surface during battery assembly or cycling [41, 42]. Researchers have tried to combat this by bonding the ceramics onto the membrane surface, which can be time and cost consuming [43]. These results show that we are able to maintain a ceramic-rich surface without the use of expensive post-treatment techniques.

Conclusion

We have successfully created a PAN/PDC hybrid nanofiber using the electrospinning method. Fiber membranes that were created had an average thickness of 27 μm, with porosity averaging 80%. TEM images confirmed that the PDC is well distributed within the fiber, forming an interconnected ceramic network within the fiber, while a thin sheath layer of ceramic is observed on the fiber surface. Incorporation of PDC in the PAN leads to an increase in both thermal and mechanical stabilities over the pristine fiber. Additionally, there was a decrease in contact angle between the membranes and electrolyte and an increase in electrolyte uptake leading to an increase in ionic conductivity. Over 100 cycles, despite the doubling the porosity (41% vs. 82%), the performance of PAN nanofiber separator at 0.2C (86% retention) was very close to that of Celgard (85% retention), suggesting that Li-ion transfer through the pores may not a deciding factor to enhance the performance of the separator. On the contrary, the PAN/PDC membranes demonstrated increased initial discharge capacity and capacity retention compared to the PAN compound and Celgard, especially at high charge/discharge rates. All nanofiber-based separators in the current study have the similar porosity around 80%,

and they exhibit a wide range of the rate capability performances due to their unique internal and surface morphologies. These results suggest that the increased ionic conductivity and wetting behavior by both the ceramics within the membrane and on the surface of the membrane are more correlated to an increase in battery performance and capacity retention than the porosity. Further work to investigate the effect of each component (contribution of internal and surface morphology) on battery performance is currently underway.

Acknowledgement

Funding was provided by AZ Electronic Materials (Cornell OSP No. 70529), and Axium Nanofibers (Cornell OSP No. 70530).

References

[1] Arora P, Zhang Z (2004) Battery separators. Chem Rev 104:4419–4462. doi:10.1021/cr020738u

[2] Huang X (2010) Separator technologies for lithium-ion batteries. J Solid State Electrochem 15:649–662. doi:10.1007/s10008-010-1264-9

[3] Zhang SS (2007) A review on the separators of liquid electrolyte Li-ion batteries. J Power Sources 164:351–364. doi:10.1016/j.jpowsour.2006.10.065

[4] Cavaliere S, Subianto S, Savych I et al (2011) Electrospinning: designed architectures for energy conversion and storage devices. Energy Environ Sci 4:4761–4785. doi:10.1039/C1EE02201F

[5] Ryou M-H, Lee DJ, Lee J-N et al (2012) Excellent cycle life of lithium-metal anodes in lithium-ion batteries with mussel-inspired polydopamine-coated separators. Adv Energy Mater 2:645–650. doi:10.1002/aenm.201100687

[6] Miao J, Miyauchi M, Simmons TJ et al (2010) Electrospinning of nanomaterials and applications in electronic components and devices. J Nanosci Nanotechnol 10:5507–5519

[7] Costa CM, Nunes-Pereira J, Rodrigues LC et al (2013) Novel poly(vinylidene fluoride-trifluoroethylene)/poly(-ethylene oxide) blends for battery separators in lithium-ion applications. Electrochim Acta 88:473–476. doi:10.1016/j.electacta.2012.10.098

[8] Yanilmaz M, Lu Y, Li Y, Zhang X (2015) SiO_2/polyacrylonitrile membranes via centrifugal spinning as a separator for Li-ion batteries. J Power Sources 273:1114–1119. doi:10.1016/j.jpowsour.2014.10.015

[9] Jiang H, Ge Y, Fu K et al (2014) Centrifugally-spun tin-containing carbon nanofibers as anode material for lithium-ion batteries. J Mater Sci 50:1094–1102. doi:10.1007/s10853-014-8666-5

[10] Vazquez B, Vasquez H, Lozano K (2012) Preparation and characterization of polyvinylidene fluoride nanofibrous membranes by forcespinning™. Polym Eng Sci 52:2260–2265. doi:10.1002/pen.23169

[11] Weng B, Xu F, Alcoutlabi M et al (2015) Fibrous cellulose membrane mass produced via forcespinning® for lithium-ion battery separators. Cellulose 22:1311–1320. doi:10.1007/s10570-015-0564-8

[12] Lee J, Lee C-L, Park K, Kim I-D (2014) Synthesis of an Al2O3-coated polyimide nanofiber mat and its electrochemical characteristics as a separator for lithium ion batteries. J Power Sources 248:1211–1217. doi:10.1016/j.jpowsour.2013.10.056

[13] Zhang L, Aboagye A, Kelkar A et al (2013) A review: carbon nanofibers from electrospun polyacrylonitrile and their applications. J Mater Sci 49:463–480. doi:10.1007/s10853-013-7705-y

[14] Qiu Y, Geng Y, Yu J, Zuo X (2013) High-capacity cathode for lithium-ion battery from $LiFePO_4$/(C + Fe_2P) composite nanofibers by electrospinning. J Mater Sci 49:504–509. doi:10.1007/s10853-013-7727-5

[15] Yanilmaz M, Zhang X (2015) Polymethylmethacrylate/polyacrylonitrile membranes via centrifugal spinning as separator in Li-ion batteries. Polymers 7:629–643. doi:10.3390/polym7040629

[16] Hao J, Lei G, Li Z et al (2013) A novel polyethylene terephthalate nonwoven separator based on electrospinning technique for lithium ion battery. J Membr Sci 428:11–16. doi:10.1016/j.memsci.2012.09.058

[17] Cho T-H, Tanaka M, Onishi H et al (2008) Battery performances and thermal stability of polyacrylonitrile nano-fiber-based nonwoven separators for Li-ion battery. J Power Sources 181:155–160. doi:10.1016/j.jpowsour.2008.03.010

[18] Jung H-R, Ju D-H, Lee W-J, Zhang X (2009) Electrospun hydrophilic fumed silica/polyacrylonitrile nanofiber-based composite electrolyte membranes. Electrochim Acta 54:3630–3637. doi:10.1016/j.electacta.2009.01.039

[19] Yang C, Jia Z, Guan Z, Wang L (2009) Polyvinylidene fluoride membrane by novel electrospinning system for separator of Li-ion batteries. J Power Sources 189:716–720. doi:10.1016/j.jpowsour.2008.08.060

[20] Liang Y, Cheng S, Zhao J et al (2013) Heat treatment of electrospun Polyvinylidene fluoride fibrous membrane separators for rechargeable lithium-ion batteries. J Power Sources 240:204–211. doi:10.1016/j.jpowsour.2013.04.019

[21] Jeon KS, Nirmala R, Navamathavan R et al (2014) The study of efficiency of Al_2O_3 drop coated electrospun meta-aramid nanofibers as separating membrane in lithium-ion secondary batteries. Mater Lett 132:384–388. doi:10.1016/j.matlet.2014.06.117

[22] Miao Y-E, Zhu G-N, Hou H, Xia Y-Y (2013) Electrospun polyimide nanofiber-based nonwoven separators for lithium-ion batteries. J Power Sources 226:82–86. doi:10.1016/j.jpowsour.2012.10.027

[23] Gopalan AI, Santhosh P, Manesh KM et al (2008) Development of electrospun PVdF–PAN membrane-based polymer electrolytes for lithium batteries. J Membr Sci 325:683–690. doi:10.1016/j.memsci.2008.08.047

[24] Cho TH, Sakai T, Tanase S, Kimura K (2007) Electrochemical performances of polyacrylonitrile nanofiber-based nonwoven separator for lithium-ion battery. Electrochem Solid-State Lett 10:A159. doi:10.1149/1.2730727

[25] Choi E-S, Lee S-Y (2011) Particle size-dependent, tunable porous structure of a SiO_2/poly(vinylidene fluoride-hexafluoropropylene)-coated poly(ethylene terephthalate) nonwoven composite separator for a lithium-ion battery. J Mater Chem 21:14747–14754. doi:10.1039/C1JM12246K

[26] Jeong H-S, Choi E-S, Lee S-Y (2012) Composition ratio-dependent structural evolution of SiO_2/poly(vinylidene fluoride-hexafluoropropylene)-coated poly(ethylene terephthalate) nonwoven composite separators for lithium-ion batteries. Electrochim Acta 86:317–322. doi:10.1016/j.electacta.2012.03.126

[27] Liu H, Xu J, Guo B, He X (2014) Effect of Al_2O_3/SiO_2 composite ceramic layers on performance of polypropylene separator for lithium-ion batteries. Ceram Int 40:14105–14110. doi:10.1016/j.ceramint.2014.05.142

[28] Jeong H-S, Hong SC, Lee S-Y (2010) Effect of microporous structure on thermal shrinkage and electrochemical performance of Al_2O_3/poly(vinylidene fluoride-hexafluoropropylene) composite separators for lithium-ion batteries. J Membr Sci 364:177–182. doi:10.1016/j.memsci.2010.08.012

[29] Jeong H-S, Choi E-S, Lee S-Y, Kim JH (2012) Evaporation-induced, close-packed silica nanoparticle-embedded nonwoven composite separator membranes for high-voltage/high-rate lithium-ion batteries: advantageous effect of highly percolated, electrolyte-philic microporous architecture. J Membr Sci 415–416:513–519. doi:10.1016/j.memsci.2012.05.038

[30] Liu H, Xu J, Guo B, He X (2014) Preparation and performance of silica/polypropylene composite separator for lithium-ion batteries. J Mater Sci 49:6961–6966. doi:10.1007/s10853-014-8401-2

[31] Choi J-A, Kim SH, Kim D-W (2010) Enhancement of thermal stability and cycling performance in lithium-ion cells through the use of ceramic-coated separators. J Power Sources 195:6192–6196. doi:10.1016/j.jpowsour.2009.11.020

[32] Huang X, Bahroloomi D, Xiao X (2013) A multilayer composite separator consisting of non-woven mats and ceramic particles for use in lithium ion batteries. J Solid State Electrochem 18:133–139. doi:10.1007/s10008-013-2254-5

[33] Huang X (2011) Development and characterization of a bilayer separator for lithium ion batteries. J Power Sources 196:8125–8128. doi:10.1016/j.jpowsour.2011.05.054

[34] Ji L, Zhang X (2008) Ultrafine polyacrylonitrile/silica composite fibers via electrospinning. Mater Lett 62:2161–2164. doi:10.1016/j.matlet.2007.11.051

[35] Naffakh M, Díez-Pascual AM (2014) Thermoplastic polymer nanocomposites based on inorganic fullerene-like nanoparticles and inorganic nanotubes. Inorganics 2:291–312. doi:10.3390/inorganics2020291

[36] Choi SW, Kim JR, Jo SM, Lee WS (2005) Electrochemical and spectroscopic properties of electrospun PAN-based fibrous polymer electrolytes. J Electrochem Soc 152:A989–A995. doi:10.1149/1.1887166

[37] Li J, Huang X, Chen L (2000) X-ray diffraction and vibrational spectroscopic studies on PAN–LiTFSI polymer electrolytes. J Electrochem Soc 147:2653–2657. doi:10.1149/1.1393585

[38] Chung SH, Wang Y, Persi L et al (2001) Enhancement of ion transport in polymer electrolytes by addition of nanoscale inorganic oxides. J Power Sources 97–98:644–648. doi:10.1016/S0378-7753(01)00748-0

[39] Croce F, Appetecchi GB, Persi L, Scrosati B (1998) Nanocomposite polymer electrolytes for lithium batteries. Nature 394:456–458. doi:10.1038/28818

[40] Xu L, Xu F, Chen F et al (2011) Improvement in comprehensive properties of poly(methyl methacrylate)-based gel polymer electrolyte by a core-shell poly(methyl methacrylate)-grafted ordered mesoporous silica. J Nanomater 2012:e457967. doi:10.1155/2012/457967

[41] An M-Y, Kim H-T, Chang D-R (2014) Multilayered separator based on porous polyethylene layer, Al_2O_3 layer, and electro-spun PVdF nanofiber layer for lithium batteries. J Solid State Electrochem 18:1807–1814. doi:10.1007/s10008-014-2412-4

[42] Huang X, Hitt J (2013) Lithium ion battery separators: development and performance characterization of a composite membrane. J Membr Sci 425–426:163–168. doi:10.1016/j.memsci.2012.09.027

[43] Zhu X, Jiang X, Ai X et al (2015) A highly thermostable ceramic-grafted microporous polyethylene separator for safer lithium-ion batteries. ACS Appl Mater Interfaces 7:24119–24126. doi:10.1021/acsami.5b07230